Synthesis, characterization and catalysis of SAPO-56 and MAPSO-56 molecular sieves

Peng Tian, Zhongmin Liu, Lei Xu and Chenglin Sun
(Natural Gas Utilization & Applied Catalysis Laboratory, Dalian Institute of Chemical Physics, Chinese Academy of Sciences, P. O. Box 110, Dalian 116023, China)

Using N,N,N',N'-tetramethyl-1,6-hexandiammine as organic template, SAPO-56 and its metal-containing silicoaluminophosphates (M=Co, Mn and Zr) were synthesized hydrothermally. The synthesis phase diagram and crystallization kinetics of SAPO-56 were obtained. The synthesis regulation of pure MAPSO-56 molecular sieves was also investigated. The samples were characterized by XRD, SEM, TG-DTA and MAS NMR. SAPO-56 and MAPSO-56 were studied with respect to their catalytic behaviors in the methanol-to-olefins conversion and the oxidation of alkane, respectively.

1. INTRODUCTION

Silicoaluminophosphate molecular sieve (SAPOs)[1,2] have attracted considerable interests because they can be used as ion exchangers, adsorbents and catalysts. According to recent papers and publications, several SAPO-n materials have potential applications in petrochemical conversion processes[3,4,5]. Furthermore, metal-containing silicoaluminophosphate (MAPSOs)[6,7] are also attracting, which have showed some specific properties and catalytic activity due to the incorporation of metals.

SAPO-56, first reported by Wilson and coworkers[8,9], has novel topology (ATX). It has an unique three-dimension structure of 8-ring channels and the pore diameter is 0.34×0.36nm. As a novel microporous silicoaluminophosphate molecular sieve, the information about the synthesis regulation and fundamental physico-chemical properties of SAPO-56 has not been found in the public report. The present paper describes the synthesis of SAPO-56 and MAPSO-56 (M=Co, Mn and Zr) in detail. The samples' physicochemical properties and their use as catalysts for methanol-to-olefins conversion and alkane oxidation reaction were also investigated.

2. EXPERIMENTS

2.1. Synthesis

SAPO-56 and MAPSO-56 were synthesized hydrothermally using N,N,N',N'-tetramethyl-1,6-hexandiammine (TMHD) as organic template. The starring material were

pesudoboehmite, phosphoric acid (85%), silica gel (25%), $Me(CH_3COO)_2$, TMHD (self synthesized) and deionized water. Under stirring, phosphoric acid, a half of water, pesudoboehmite, silica gel, a half of water and TMHD were added to a beaker in turn. The resulting gel was sealed in an stainless steel reactor and heated in an oven at 200°C for 48h. MAPSO-56 was synthesized as same as SAPO-56. Metal sources were added after the addition of silica gel. The final solid product was filtered, washed and dried at 200°C for 24h. Three samples of SAPO-56 were synthesized specially for characterization and catalytic tests. Their gel and product compositions were showed in table 1. The typical starting compositions of pure MAPSO-56 (M=Co, Mn and Zr) were also presented in the same table.

Table 1
Gel and product compositions of SAPO-56 and MAPSO-56 (M=Co, Mn and Zr)

Sample	Gel compositions						Product composition (mol)		
	Al_2O_3	P_2O_5	SiO_2	MeO	TMHD	H_2O	Al	P	Si
SAPO-56/A	1	1	0.4	0	2	50	0.516	0.349	0.135
SAPO-56/B	0.8	1	0.6	0	2	50	0.478	0.334	0.188
SAPO-56/C	0.72	0.72	0.92	0	2	50	0.414	0.282	0.303
CoAPSO-56	0.8	1	0.6	0.06	2	50	-	-	-
MnAPSO-56	0.8	1	0.6	0.06	2	50	-	-	-
ZrAPSO-56	0.8	1	0.6	0.06	2	50	-	-	-

2.2. Characterization

X-ray powder diffraction (XRD) was recorded on Rigaku instrument (Model D/Max-γB) using Cu-Kα radiation, filtered through a nickel foil. Element analysis was carried out by XRF using Bruk SRS 3400. The SEM photograph of SAPO-56 was taken on a Hitachi S-3200N microscope. Thermal analysis (TG, DTA) were carried out in air on a Shimadu DT-30 thermal analyzer. The as-synthesized sample was heated from 15°C to 1200°C at a rate of 10°C/min. ^{29}Si, ^{31}P and ^{27}Al MAS NMR spectra were carried out on a Bruker DRX-400 spectrometer. Spinning speeds were 4k, 4k, and 8kHz for ^{29}Si, ^{31}P, and ^{27}Al, respectively, and chemical shifts are quoted respectively from DDS (3-Trimethylsiyl propanesulfonic acid sodium salt), 85% phosphoric acid, and $Al(H_2O)_6^{3+}$. Short radio-frequency pulses 1/20 was used for the ^{27}Al spectra to ensure that the measurements were quantitatively reliable.

2.3. Catalytic tests

Before each catalytic run the as-synthesized molecular sieve was calcined at 550°C for 4h to get rid of the template.

Methanol-to-olefins conversion was determined in a fixed bed connected to a gas chromatograph. 1.5g of catalyst (calcined, 20~40 mesh) was loaded in the reactor. The catalyst was first activated at 500°C in N_2 for 1h. Then the temperature fell to 450°C (reaction temperature). Methanol was fed using N_2. The N_2 flow was 65 ml/min and the WHSV of methanol was $2.0h^{-1}$.

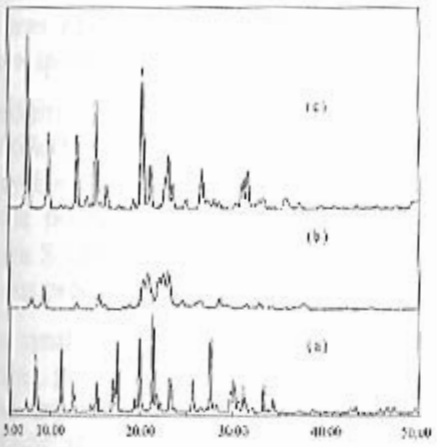

Fig. 1 XRD patterns
(a) SAPO-56 (b) SAPO-11 (c) $AlPO_4$-17

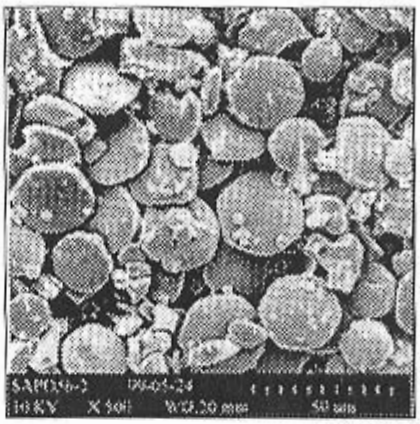

Fig.2 SEM photograph of SAPO-56

The oxidation reaction was performed in a 100-ml autoclave lined with polytetrafluoroethylene. Typically, 1.0g of the catalyst (calcined) and 20g of alkane were introduced into the reactor. The reactor was charged with 11atm O_2 and heated to 120°C for 23h. Oxygen was fed continuously to maintain a constant O_2 concentration. The quantitative analyses was carried out by GC with a capillary column (FFAP, 30m×0.25mm).

3. RUSULTS AND DISCUSSIONS

3.1. Synthesis of SAPO-56 and MAPSO-56

Fig 1 (a) shows the XRD pattern of as-synthesized SAPO-56/A which was in accordance with the literature[9]. The SEM photograph of the same sample is given in Fig 2, which reveals that the crystals were flat hexagonal morphology. By fixed the amount of TMHD and H_2O in the gel [n(H2O)/n(TMHD)=9.5, n(TMHD)/n(Si+Al+P)=0.48, 200°C,48h], we obtained the Al_2O_3-SiO_2-P_2O_5 ternary phase diagram of SAPO-56 (Fig. 3). From Fig. 3, it could be observed that the pure phase area of SAPO-56 appeared in the region of $0.5<n(SiO_2)/n(M)<0.7$ ($M = SiO_2+Al_2O_3+P_2O_5$) $0.15<n(Al_2O_3)/n(M)<0.4$ and $0.1<n(P_2O_5)/n(M)<0.3$ in the phase diagram. In the other area of the diagram phase, pure SAPO-56 could also be

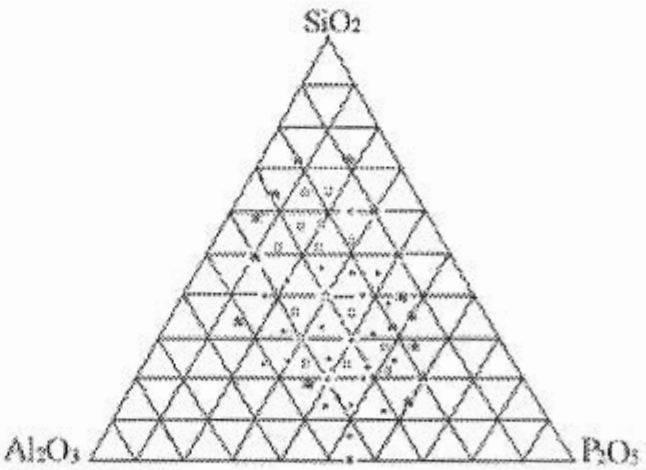

Fig. 3 Ternary phase diagram of SAPO-56
□ - SAPO-56 * - amorphous phase
● - SAPO-56 containing other crystals
■ - $AlPO_4$-17

synthesized, but in most cases SAPO-56 containing other crystals appeared. When the silica content was zero, only pure $AlPO_4$-17 was obtained (Fig 1, c). So it can be concluded that high silica in the gel benefited the synthesis of SAPO-56.

In addition, a minimum amount of TMHD [n(TMHD)/n(P_2O_5)≥2, xTMHD: 0.8Al_2O_3: P_2O_5: 0.6SiO_2: 50H_2O, 200°C, 48h] in the silicoaluminophosphate gel was found to be necessary for obtaining pure SAPO-56. If the n (TMHD)/n (P_2O_5) ratio was in the range of 0.6~2, the product was SAPO-56 together with SAPO-11. When n(TMHD)/n(P_2O_5) ratio ≤0.5, pure SAPO-11 appeared (Fig.1 b). If the n(TMHD)/n(P_2O_5) ratio was lower than 0.5, amorphous products became dominant.

The synthesis of MAPSO-56 was observed strongly dependent on the metal amount of the starting gel (2 TMHD: 0.8 Al_2O_3: P_2O_5: 0.6 SiO_2: 50 H_2O, 200°C, 48h). ZrAPSO-56 could be crystallized in a wide range of n (Zr)/n (P_2O_5) ratio from 0.02 to 0.18. Pure CoAPSO-56 and MnAPSO-56 only appeared below n (Me)/n (P_2O_5) ratio of 0.06.

3.2. Kinetics of crystallization

The crystallization curve of SAPO-56/A is presented in Fig 4. The crystallinity was calculated by averaging the five strongest peaks of each sample's XRD pattern. It can be seen that there were few crystals after 5h. The crystallinity increased rapidly with time during 5~9h and reached 100% at 9h. This implied that SAPO-56 had the characterization of rapid crystallization. However, the crystals were very small at this time. With the increase of time, the crystals grew big. It was interesting to note that after 9h the relative crystallization of the sample would decrease with crystallization time. During 14~72h, the crystallinity of SAPO-56 kept constant. After 72h, the relative crystallization decreased obviously and XRD showed that amorphous phase appeared.

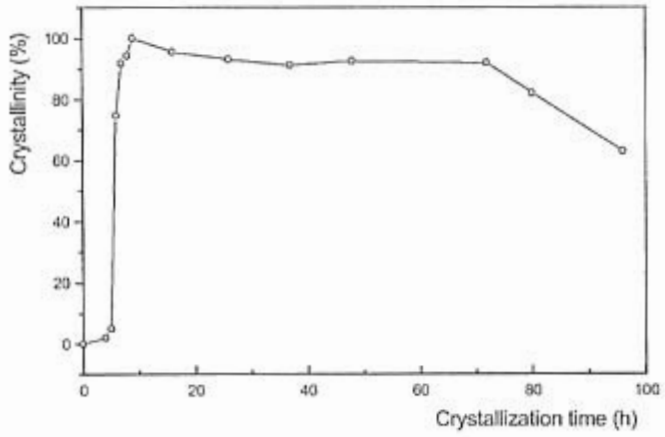

Fig. 4 The crystallization curve of SAPO-56

3.3. Thermal analysis

Fig 5 shows the TG and DTA of SAPO-56/A sample. In the low-temperature region up to 260°C, there was an endothermic weight loss of 4.4%, due to the lose of physisorption water. In the temperature region of 260°Cto 660°C, there were two stages of exothermic weight loss (5.7% and 8.6%), due to the oxidative decomposition of the template occluded in the sample. Furthermore, there appeared an exothermic peak at 1130°C in the DTA curve and no weight loss could be observed at the corresponding position of the TG curve. So it can be inferred that the peak at 1130°C corresponded to the collapse of the framework.

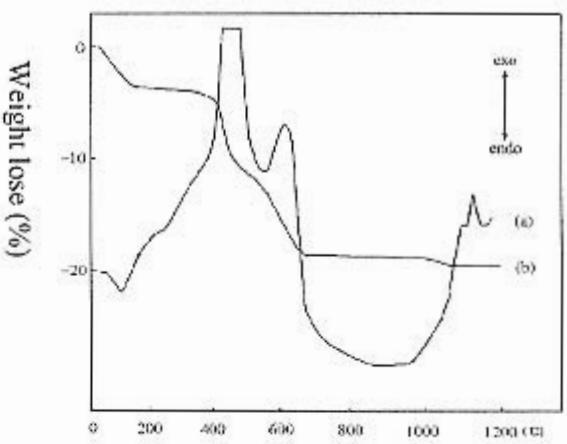

Fig.5 TG and DTA patterns of SAPO-56
(a) DTA curve (b) TG curve

3.4. MAS NMR

Fig 5 shows ^{29}Si, ^{27}Al and ^{31}P MAS NMR spectra of the as-synthesized SAPO-56/A, SAPO-56/B and SAPO-56/C samples. The chemical shift of –92ppm in the ^{29}Si MAS NMR could be assigned to Si(4Al) and peaks between –94ppm and –111ppm were attributed to different silicon substituted environment in the framework. SAPO-56/A gave one strong peak at –92ppm and one weak peak at –96ppm, which suggested most of the silicon was present in the Si(4Al) environment and a very few silicon appeared in the Si(3Al) environment. Following the increase of silicon content, these peaks between –94 and –111ppm became obvious. Besides peaks at –92 and –96ppm, SAPO-56/B shows peaks at around –96 and –101ppm which can be assigned to Si(3Al) and Si(2Al), respectively. The proportion of Si(0Al) was very large in SAPO-56/C sample. In view of the results of element catalysis which showed the silicon content was very high, two explanations for Si(0Al) are possible : silica island in the framework and amorphous silica.

The ^{31}P MAS NMR spectra show a single symmetrical line at –28ppm, which can be assigned to a single P(4Al) environment irrespectively of the amount of silicon. This is in accordance to the known fact that P-O-Si linkages are absent in the SAPO materials. The ^{27}Al MAS NMR gave two resonances at 39 and 8.7ppm. The chemical shift of 39ppm may arise from aluminum in tetrahedral environment. We ascribed the peak at 8.7ppm to additional coordination of aluminum with organic template or water, considering the similar observations in the case of SAPO-34 and SAPO-44[10,11] etc.

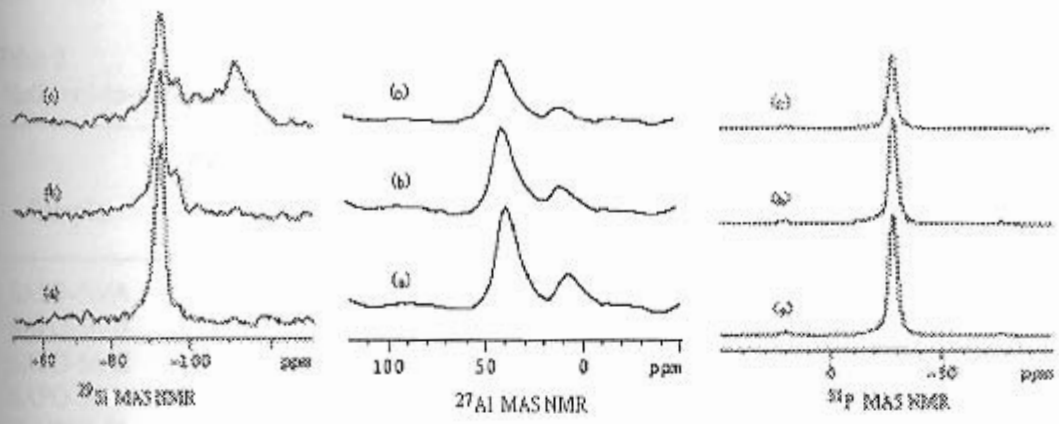

Fig. 6 ^{29}Si, ^{27}Al and ^{31}P MAS NMR spectra of the as-synthesized SAPO-56
(a) SAPO-56/A (b) SAPO-56/B (c) SAPO-56/C

3.5. Catalytic test

The results of the methanol-to-olefins conversion are presented in table 2. For comparison, SAPO-34 molecular sieve was also tested under the same condition and its result was showed in the same table. It can be seen that the activity and selectivity to light olefins decreased gradually, following the increase of silicon in the SAPO-56 samples. ^{29}Si MAS NMR spectra showed that the proportion of Si(4Al) and Si(3Al) decreased from SAPO-56/A to SAPO-56/C. The environment of Si(4Al) and Si(3Al) in the molecular sieves probably benefited the reaction. The pore size of SAPO-56 is smaller than that of SAPO-34, but the selectivity to light olefins didn't show any superiority on SAPO-56. So it can be inferred that the pore diameter wasn't the determinant factor to the selectivity. Moreover, Co-, MnAPSO-56 also exhibited good catalytic properties in this reaction, while ZrAPSO-56 showed poor catalytic behavior. It implies that the addition of metal to the molecular sieve can have a remarkable effect on the reaction. However, SAPO-56 and MAPSO-56 deactivated rapidly with reaction time and after 30min nearly all of the samples lost their activity. The rapid deactivation of SAPO-56 and MAPSO-56 may be due to their large accessible cages and small pore size. The product of high C/H ratio formed in the reaction can't diffuse from the interior of the molecular sieves.

Transition metal containing SAPO-56 was found to be oxidation catalyst for alkane transformation at low temperature. The results of n-octane oxidation on MAPSO-56 were indicated in table 3. From the table 3, it can be seen that the products consisted of 2,3,4-octanone, 2,3,4-octanol, cracked oxygenates and oxygenates with more than one functional group. Co- and Mn-containing SAPO-56 showed higher oxidation activities than ZrAPSO-56. In all cases no terminal oxidation products were detected, suggesting that the oxidation reaction took place only on the external surface of MAPSO-56.

Table 2
Methanol-to-olefins conversion over SAPO-56 and SAPO-34 catalysts

Sample	Methanol conversion* (%)	Product distribution (wt%)							
		CH_4	C_2H_4	C_2H_6	C_3H_6	C_3H_8	$C_4^=+C_4^0$	$C_5^=+C_5^0$	$C_2^=+C_3^=$
SAPO-56/A	100	3.1	35.2	0.4	35.0	11.1	9.5	5.7	70.2
SAPO-56/B	70.1	2.5	32.9	0.6	32.0	8.0	17.3	6.7	64.9
SAPO-56/C	34.0	4.2	31.8	0.9	32.8	4.8	7.9	17.6	64.6
SAPO-34	100	1.0	53.7	0.3	35.5	-	-	-	81.3
ZrAPSO-56	6.3	15.6	50.0	3.1	31.3	-	-	-	81.3
MnAPSO-56	100	4.4	34.6	1.4	30.3	16.0	10.8	2.5	64.9
CoAPSO-56	100	5.4	30.2	1.2	20.8	27.4	11.2	3.7	51.0

*Methanol conversion = $X/[X+2M(Me_2O)+M(MeOH)]$
$X=M(CH_4)+\sum nM(C_nH_{2n})+\sum nM(C_nH_{2n+2})$, n=2~5; Reaction time=1.5 minute

Table 3
N-octane oxidation reaction on MeAPSO-56 molecular sieves

Sample	Conversion (mol%)	Product distribution (wt%)						
		2-one	3-one	4-one	2-ol	3-ol	4-ol	others*
ZrAPSO-56	5.7	19.6	15.6	14.5	8.3	6.3	5.8	29.9
CoAPSO-56	8.3	19.0	15.1	13.2	10.7	9.2	8.3	24.4
MnAPSO-56	8.6	18.2	14.8	13.9	8.2	6.7	5.9	32.3

*others = most cracked oxygenates and few oxyenates with more than one functional group

4. CONCLUSIONS

SAPO-56 and MAPSO-56 were synthesized successfully. The pure phase area of SAPO-56 appeared in the range of $0.5<n(SiO_2)/n(M)<0.7$ ($M=SiO_2+Al_2O_3+P_2O_5$)□$0.15<n(Al_2O_3)/n(M)<0.4$ and $0.1<n(P_2O_5)/n(M)<0.3$ in the Al_2O_3-SiO_2-P_2O_5 ternary phase diagram. Co- and Mn-containing SAPO-56 could be synthesized in low Me/P_2O_5 ratio of 0.06, while pure ZrAPSO-56 appeared in a wide Zr/P_2O_5 ratio from 0.02 to 0.18. Thermal analysis showed that SAPO-56 had high thermal stability. SAPO-56, Co- and MnAPSO-56 exhibited good initial activity and selectivity to light olefins. However they deactivated rapidly. In the oxidation of n-octane Co- and MnAPSO-56 showed higher activity than ZrAPSO-56.

REFERENCES

1. B. M. Lok, C. A. Messina, R. L. Patton, R. T. Gajek, T. R. Cannon and E. M. Flanigen, J.

Am. Chem. Soc., 106 (1984) 6092

2. B. M. L ok, C. A. Messina, R. L. Patton, R. T. Gajek, T. R. Cannon and E. M. Flanigen, US Patent No. 4 440871 (1984)

3. J. A. Rabo, R. J. Pellet, P. K. Coughlin and E. S. Shamshoum, Stud. Surf. Sci. Catal., 46 (1989) 1

4. J. A. Martens, P. J. Grobet and P. A. Jacobs, J. Catal., 126 (1990) 299

5. R. Wendelbo, D.Akporiaye, A. Andersen, I. M. Dahi and H. B. Mostad, Appl. Catal., A: General, 142 (1996) 197

6. S. Hocevar, J. Batista and V. Kaucic, J. Catal., 139 (1993) 351

7. R. A. Sheldon, Stud. Surf. Sci. Catal., 110 (1997), 151

8. S. T. Wilson, N. K. McGuire, C. S. Blackwell, C. A. Bateman and R. M. Kirchner, Stud. Surf. Sci. Catal., 98 (1995) 9

9. S. T. Wilson, R. W. Broach, C. S. Blackwell, C. A. Bateman, N. K. McGuire, and R. M. Kirchner, Mircoporous and Mesoporous Materials, 28 (1999) 125

10. R. B. Borade and A. Clearfield, J. Mol. Catal., 88 (1994) 249

11. S. Ashtekar, S. U. V. Chilukuri and D. K. Chakrabarty, J. Phys. Chem., 98 (1994) 4878